Cement and Concrete Research 38 (2008) 1079–1091

Contents lists available at ScienceDirect

Cement and Concrete Research

journal homepage: http://ees.elsevier.com/CEMCON/default.asp

Mechanical properties of the rust layer induced by impressed current method in reinforced mortar

S. Caré [a,*], Q.T. Nguyen [b], V. L'Hostis [c], Y. Berthaud [b]

[a] Université Paris Est, Institut Navier, LMSGC (LCPC/ENPC/CNRS), 2, allée Kepler, 77420 Champs sur Marne, France
[b] ENS Cachan/CNRS/UPMC/PRES UniverSud Paris, LMT-Cachan, 61 avenue du Président Wilson, 94235 Cachan, France
[c] CEA Saclay, DEN/DANS/DPC/SCCME/LECBA, Bât. 158, PC 25, 91191 Gif sur Yvette Cedex, France

ARTICLE INFO

Article history:
Received 23 April 2007
Accepted 18 March 2008

Keywords:
SEM
Corrosion
Mechanical properties
Steel reinforced mortar
Rust

ABSTRACT

This paper describes the mechanical effects of rust layer formed in reinforced mortar through accelerated tests of corrosion. The morphological and physico-chemical properties (composition, structures) of the corrosion system were characterized at different stages by using optical microscope and scanning electron microscope coupled with energy dispersive spectroscopy. The corrosion pattern was mainly characterized by a rust layer confined at the interface between the steel and the mortar. Expansion coefficient of rust products was determined from the rust thickness and the Faraday's law.
Furthermore, in order to understand the mechanical effects of corrosion on the damage of mortar, displacement field measurements were obtained by using digital image correlation. An analytical model (hollow cylinder subjected to inner and outer pressures) was used with a set of experimental data to deduce the time of cracking and the order of magnitude of the mechanical properties of the rust layer.

1. Introduction and objective

Corrosion of reinforcement bars is one of the major causes of the premature degradation of reinforced concrete structures. Initially, due to the alkalinity of the concrete pore solution (pH close to 13), steel rebars in concrete are protected by the presence of an oxide protective layer, called the passive layer, at the surface of the rebar. However, this protection can be broken by the destruction of the passive layer by aggressive ions (e.g. chlorides) or by an acidification of the environment in the vicinity of the rebar (e.g. carbonation) [1,2]. Under chloride attack, the passive film is damaged locally and steel starts to dissolve in these unprotected areas, so that a mix of general and (local) pitting corrosion is induced. In the case of penetration of carbon dioxide, the pH of the concrete pore solution close to the rebar decreases from 13 to 9 [3] causing general corrosion of steel. When steel rebars are depassivated, porous oxide layers are formed at the steel/concrete interface. When these products are solid, their volume is higher than that of the original metal [4]. As this volume increases, a pressure is induced around the embedded steel, and the concrete cover expands, which can lead to concrete cracking, spalling or delamination.

Given the importance and the extent of the problem, the phenomenon has received a lot of attention from scientists and engineers over the past decades. Experimental studies dedicated to the mechanical consequences on concrete (or mortar) of corrosion products growth have shown that cracking of the cover depends on several factors such as: concrete mixture proportions, concrete cover thickness, etc. [5]. Numerical modelling has also been developed ([6,7]). The authors considered damage of concrete due to expansion of rust at the rebar/concrete interface, leading to concrete cracking. Pressure induced by rust around the concrete was modelled by a fictitious thermal load applied to a thin interface representing the rust layer. In this context, the knowledge of the mechanical behaviour of the rust layer formed at the rebar/concrete interface is needed in order to have agreement between experiments and computations.

As the mechanical properties and the composition of the rust layer are not well known, some authors [6] considered that iron oxide is mainly composed of water and simply used the moduli of water for the rust layer. In this case, the bulk modulus K is equal to 2 GPa and the Poisson's ratio, ν=0.5. But they had to replace the Poisson's ratio value by a value slightly lower than 0.5 to solve numerical simulation, so that the Young's modulus E is small, but not zero ($E \approx 0.1$ GPa).

Ouglova et al. [8] have measured the Young's modulus of iron oxides from ultrasonic and mechanical measurements. These iron oxides were dried and were in a powder state. These laboratory grown oxides were similar to oxides obtained from 40-year old corroded reinforced structures. These authors have shown that the Young's modulus of these iron oxides was about 2 GPa and was dependent on their degree of compaction and hydration. These results may justify the values used in previous numerical simulations, but further studies have to be carried out.

* Corresponding author. Tel.: +33 1 40 43 54 66; fax: +33 1 40 43 54 50.
E-mail address: sabine.care@lcpc.fr (S. Caré).

0008-8846/$ – see front matter © 2008 Elsevier Ltd. All rights reserved.
doi:10.1016/j.cemconres.2008.03.016

Table 1
Mix proportions of mortar

	kg/m^3
Water	293
Cement	630
Siliceous–calcareous sand (0/4 mm)	1340
Water to cement ratio (*W*/*C*)	0.46
Cement to sand ratio (*C*/*S*)	0.47

The aim of this study was to analyse the mechanical effects of the rust layer in reinforced mortar. Rust layer was induced by accelerated corrosion tests by using the impressed current method. As shown in [9], accelerated corrosion test by impressed current is confirmed to be a valid method to study the corrosion process of steel in mortar, and its effects on the damage of mortar cover.

The physico-chemical properties (composition, structures) of the corrosion system were characterized at different stages by using optical microscope (OM) and scanning electron microscope (SEM) coupled with energy dispersive spectroscopy (EDS). X-ray diffraction (XRD) analyses were performed to obtain information on the crystalline structure of different phases constituting the corrosion products. Expansion coefficient (defined as the ratio of the volume of the corrosion products and the volume of iron) was predicted by using a modelling approach considering a three-phase material (steel/rust/mortar).

Furthermore, in order to understand the mechanical effect of corrosion on the damage of mortar, displacement field measurements were obtained by using digital correlation technique (Correli^{LMT} in [10,11]) developed at Laboratoire de Mécanique et Technologie (LMT). An analytical model (hollow cylinder subjected to inner and outer pressures) using experimental data allowed us to deduce the time of cracking and the order of magnitude of the mechanical properties of rust layer.

2. Experimental program

2.1. Specimen

The design of the studied mortar is shown in Table 1. The composition of the mortar was: a water to cement ratio (*W*/*C*) equal to 0.46 and a cement to sand ratio (*C*/*S*) equal to 0.47. The cement was a Portland cement (European grade CEM I 52.5); its mineralogical composition is given in Table 2. The aggregate in mortar was a siliceous–calcareous sand (0/4 mm). To promote the corrosion, 3.5% of NaCl by weight of cement was added to the mix. The studied mortar had a 28-day average compressive strength of 39 MPa, a splitting tensile strength of 3.3 MPa and a Young's modulus of 30 GPa [12].

The reinforcement was a plain carbon steel wire (FeE500 steel), 10 mm in diameter and 100 mm long. After being polished with abrasive papers and rinsed with distilled water, the steel surface was coated with an electric insulator, except for a length of 70 mm (with an area of about 2200 mm^2) so that only the unprotected zone may corrode under accelerated tests. After mixing, the fresh mortar was poured into a cylindrical plastic mould (60 mm in diameter and 100 mm high) where the reinforcement was previously placed along its longitudinal axis (Fig. 1). So, the thickness of the cover of the specimens amounted to 25 mm.

The specimens were then compacted for 60 s by using a vibrating table. After demoulding and before the accelerated corrosion tests, they were stored, at room temperature, in an alkaline solution (pH ≈ 13 with 1 g/L NaOH + 4.65 g/L KOH) which contained NaCl salt (30 g/L). The specimens were 6 months old at the beginning of the accelerated corrosion tests.

Table 2
Mineralogical composition of Portland cement

C3S	C2S	C3A	C4AF
61.9%	15.4%	8.8%	9.1%

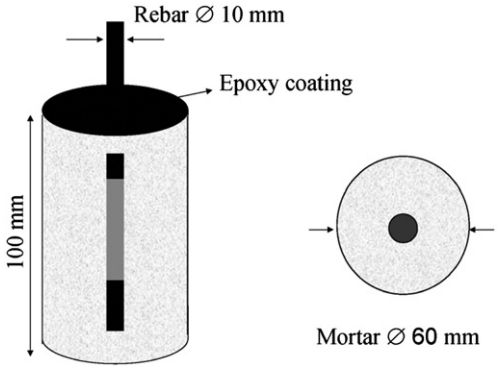

Fig. 1. Test specimen.

2.2. Accelerated corrosion tests and tests program

The accelerated corrosion tests consisted in impressing an anodic current to the rebar in order to enhance its corrosion. Fig. 2 presents the experimental set up. A power supply (6 A, 60 V) was used to apply a constant and direct current between the reinforcement and a counter-electrode, made of carbon fibre mesh and immersed in solution.

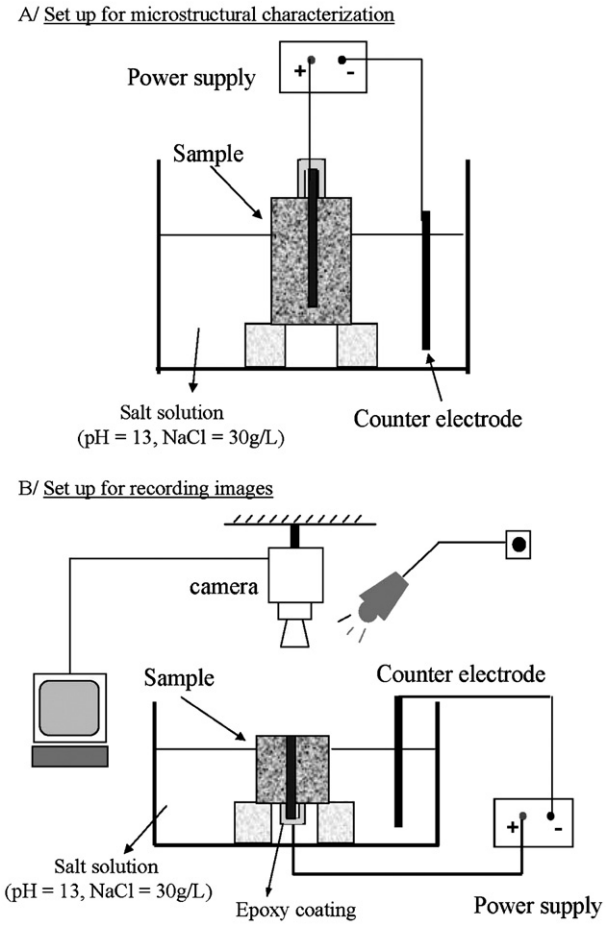

Fig. 2. Scheme of the experimental set up.

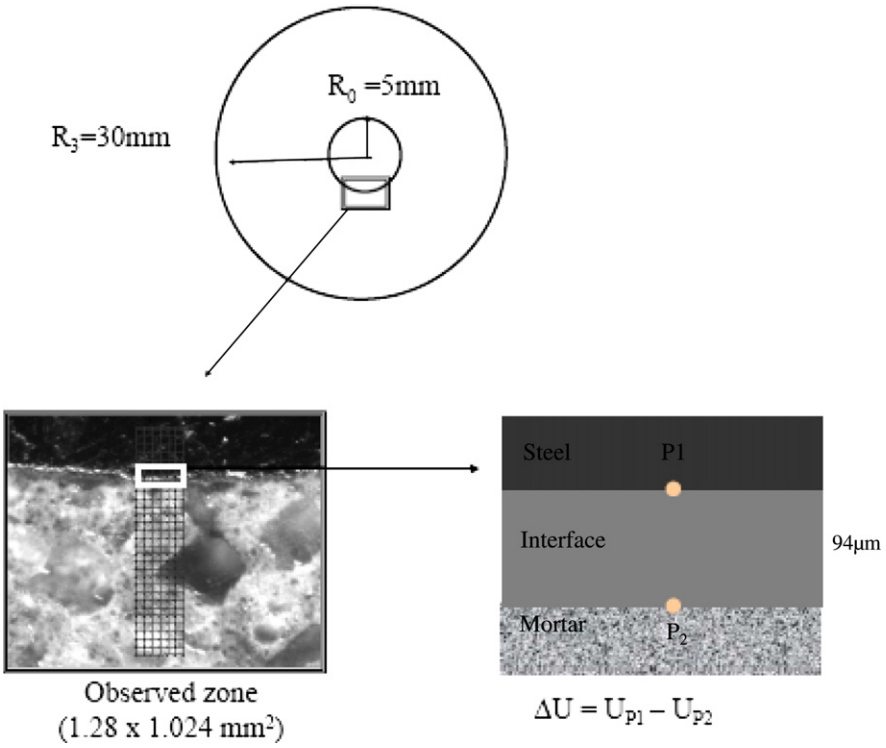

Fig. 3. Observed zone for local measurements.

In this study, samples were subjected to current density of 100 µA/cm^2. According to [4], this value allows a sufficiently short experiment, but keeps the induced corrosion within the 'natural' values which can be found in practice. A known resistance was placed in the outer electric circuit to measure the potential and then to check the magnitude of the current flowing in the system.

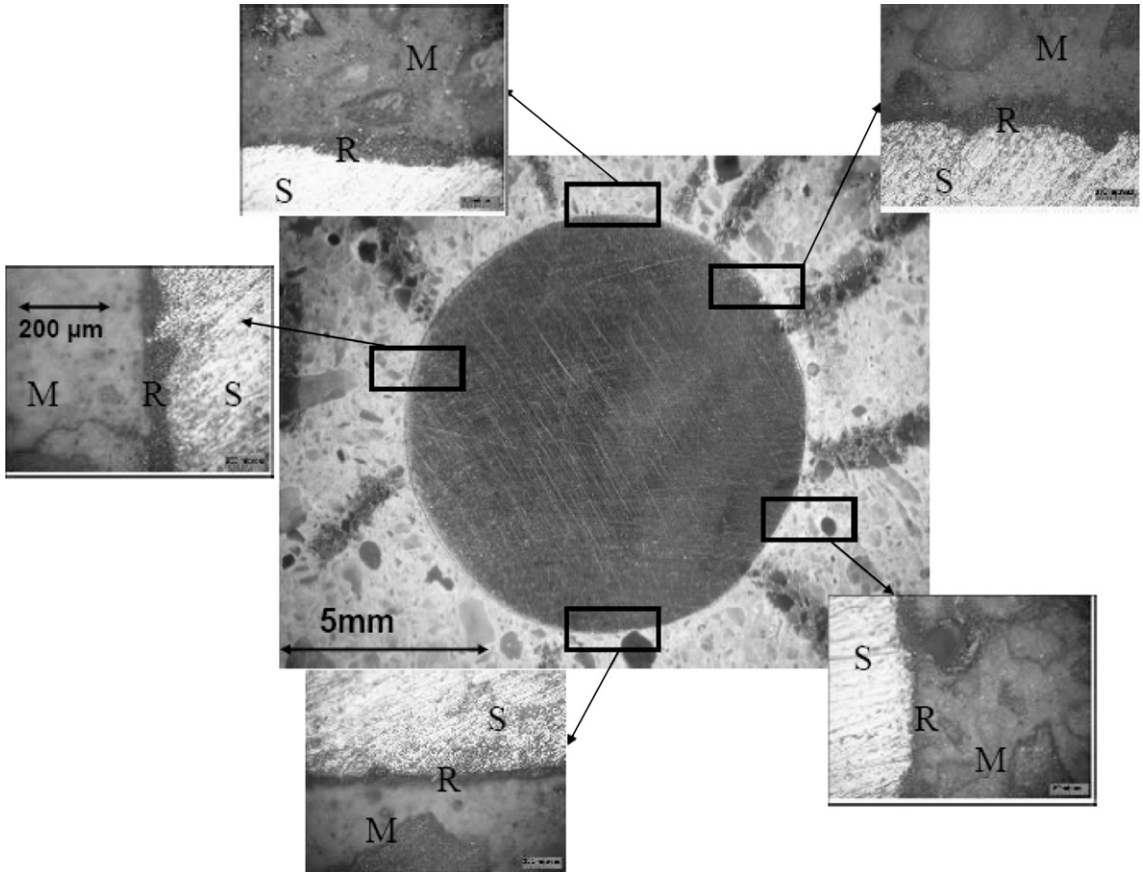

Fig. 4. OM photography of steel/mortar interface (steel diameter is 5 mm) for the sample E45. Different thicknesses for the rust layer are observed. S: steel, R: rust, M: mortar.

Two types of tests were performed: the first one allowed the characterization of the metal/mortar interface microstructure and the second one was realized in order to determine the mechanical properties of the rust.

For the first set of tests (Fig. 2A), microstructural characterization was realized at four different stages: at $t=0$ h (reference test labelled E0, before the accelerated corrosion test), and at $t=10$ h, 45 h and 76 h (tests labelled E10, E45 and E76, after the accelerated corrosion test at 10 h, 45 h and 76 h). After the accelerated corrosion tests, the specimens were cut into slices in order to analyse the corrosion pattern by microscopy in the inner reinforced mortar.

Concerning the second type of tests (Fig. 2B), the specimens were cut into two parts before the accelerated corrosion tests. A half sample was used to analyse the corrosion process by using inter-correlation image technique ([10,11]) at the upper surface. The sample was immersed partially in an aqueous solution representative of the cementitious pore solution (pH=13 with 1 g/L NaOH+4.65 g/L KOH) which contained NaCl salt (30 g/L). The upper surface of the specimen was water free to allow the recording of the digital images of the surface (Fig. 2B). Displacement and strain fields were measured continuously during 41 h.

2.3. Characterization of the corrosion system

After accelerated corrosion tests, samples were cut into slices and then ground with silicon carbide abrasive papers from grades 120 to 1000 lubricated with ethanol. Polishing was performed using ethanol to avoid modification of the rust layer during the sample preparation. An optical microscope (*Carl Zeiss*) gave a global overview of the interface between steel and mortar and allowed the thickness of the rust layer to be determined around the rebar for each stage (E0, E10, E45 and E76).

By using SEM (*Phillips L30*) with EDS analyses, chemical composition of the corrosion products was determined for two stages (E10 and E45). Finally, corrosion products reduced into powder were characterized by XRD for the stage $t=76$ h. XRD analyses were obtained on corrosion sample powders with a *Siemens D500* diffractometer for 2θ range between 5° and 90°. A cobalt anti-cathode was used (40 kV–30 mA).

2.4. Mechanical effect of rust layer

The mechanical effect of the rust layer on the mortar was analysed by using a CCD camera (Fig. 2B). The CCD camera stored images every 5 min and the pictures were analysed by using the inter-correlation

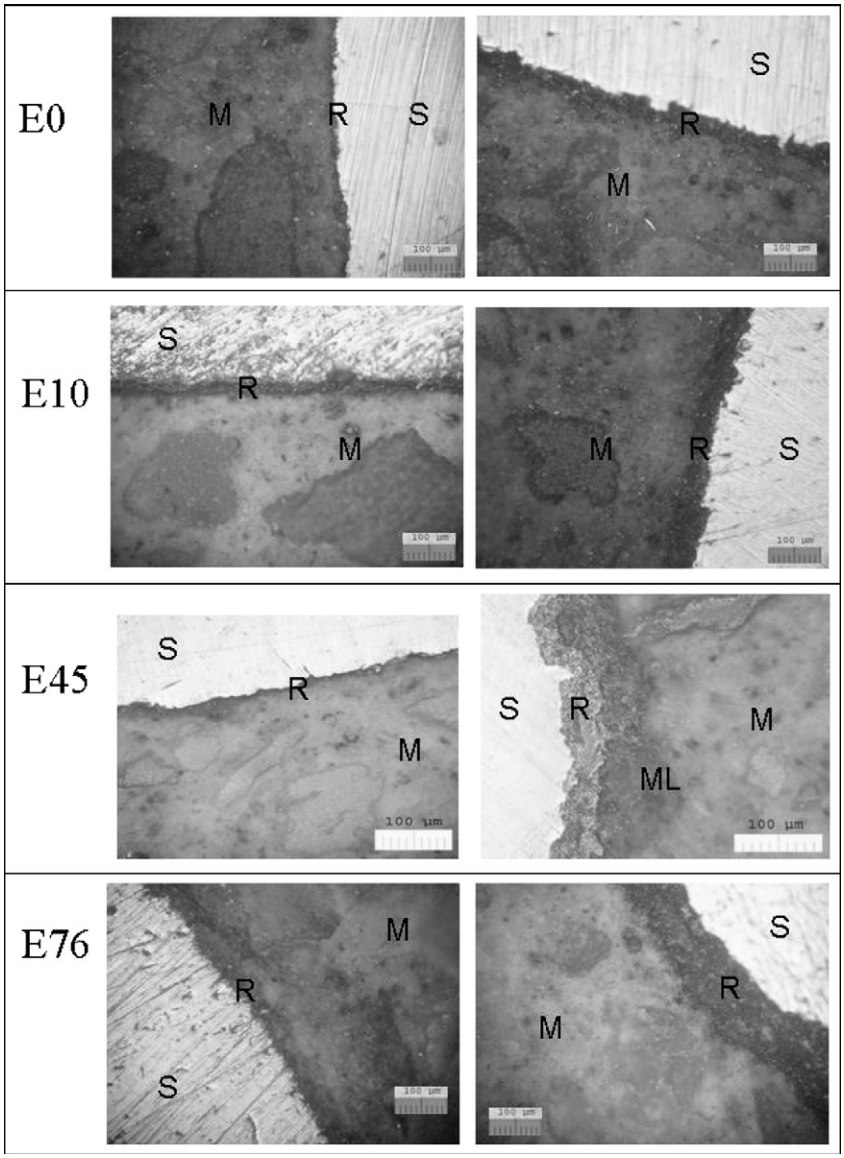

Fig. 5. Interface steel/mortar for samples EO, E10, E45 and E76 by OM. Left: Minimal thickness, right: maximal thickness. S: steel, R: rust, M: mortar, ML: mixed layer.

image technique developed at LMT ([10,11]) to derive the displacement field. The optical set up (CCD camera and ×600 magnification with long focus system) was used to observe a zone (1.28×1.024 mm^2) located at the steel/mortar interface (Fig. 3). The observed zone was a small zone around the rebar, small enough to adapt to the resolution of CCD camera and to the low values of the expected displacement (micrometers). The image taken at the beginning of the test was considered as the reference image. The analysis of displacement and strain fields by Correli^{LMT} ([10,11]) software provided information about the growth of the interface during the test.

3. Characterization of the corrosion system

3.1. Analytical characterization of the metal/mortar interface

Observations under optical microscope of samples subjected to accelerated corrosion tests allowed the characterization of the general corrosion pattern (Figs. 4 and 5). Our observations showed that:

- Close to the metal, a brown layer has been observed. Its thickness was heterogeneous around the rebar. For instance, for the sample E45, the average thickness of this interface layer was about 30 µm, with a minimum of 10 µm and a maximum of 50 µm.
- Surrounding this layer, a clearer layer was sometimes observed (named mixed layer). Its microstructure was similar to the mortar microstructure, but the brown colour let think to the presence of iron oxides.

It can be noticed that the steel rebar was corroded before accelerated tests because of the presence of NaCl in mortar. The average thickness of the rust layer for E0 was about 10 µm. The corrosion pattern (rust layer confined at the interface) was similar before (E0) and after the accelerated corrosion tests (E10, E45, E76). It is possible to conclude

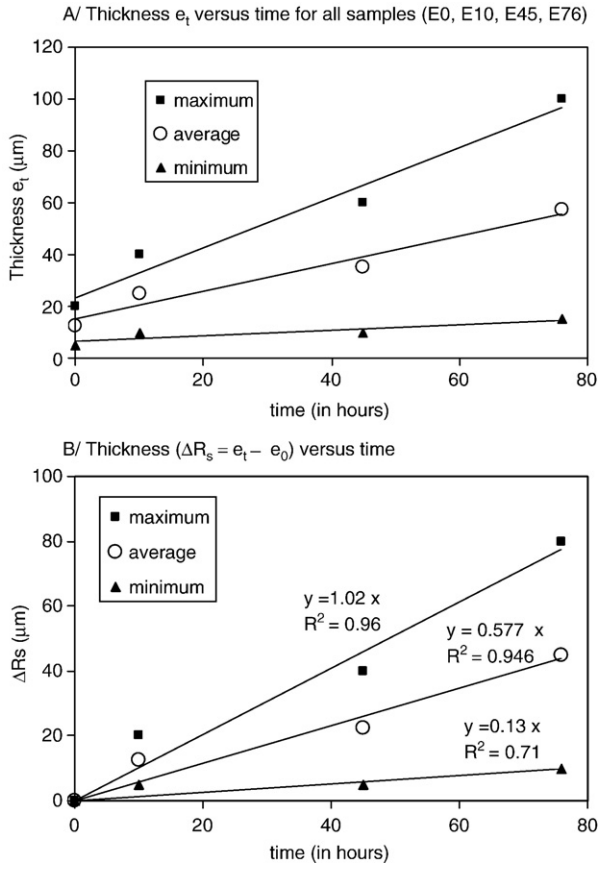

Fig. 6. Measurements of the thickness (in µm) of the rust layer against time (t in hours).

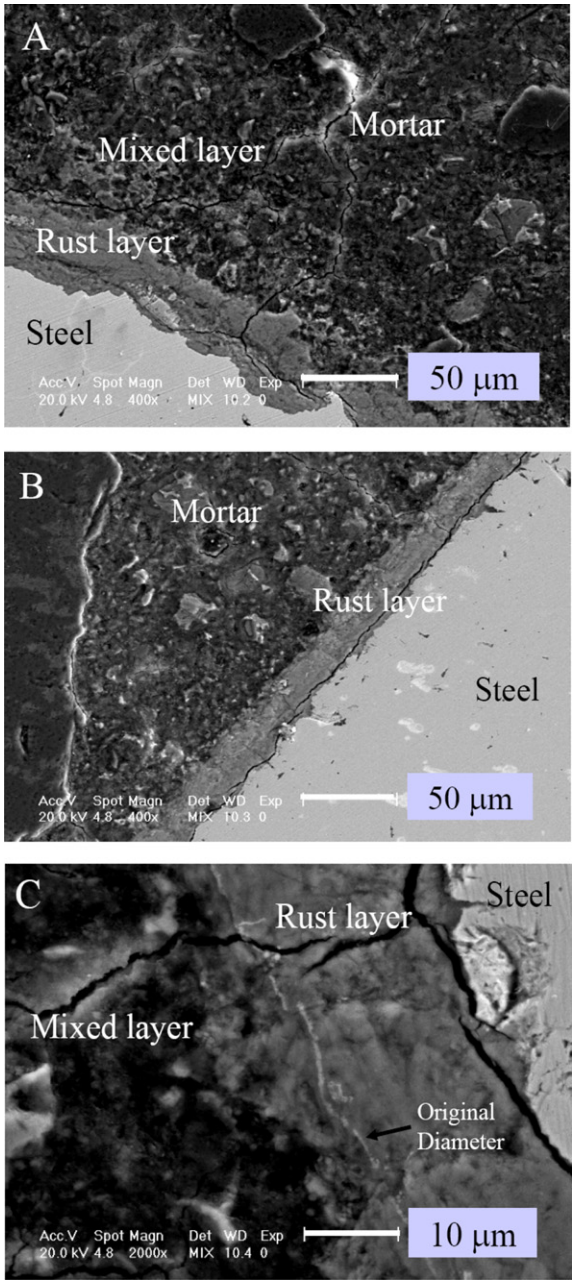

Fig. 7. SEM photographies of steel/mortar interface for sample E45. A/ Zone with rust layer and mixed layer. B/ Zone with rust layer, without mixed layer. C/ Rust layer with the possibly trace of the original rebar diameter (in this case the rust expansion coefficient given by $\eta = \frac{\Delta R_s}{X}$ is estimated to be equal to about 1.5).

that the corrosion pattern was not modified by the technique of impressed current. Furthermore, no pitting due to chloride was observed so that we can consider a general corrosion process (Fig. 5).

Rust thickness was measured on samples subjected to corrosion during 0, 10, 45 and 76 h. One slice was observed and several measurements were made around the rebar to take into account the heterogeneity of corrosion around the rebar. The corrosion pattern is assumed to be the same along the rebar. Results (Fig. 6A) showed that the thickness increased with the duration of the tests. Considering that the steel rebar was corroded during the curing step due to the presence of chlorides in mortar, the average change in thickness (ΔR_s) during accelerated tests was determined. The average thickness was defined by $\Delta R_s = e_t - e_0$ where e_t was the thickness measured at the time t (t=0, 12, 45, 76 h) and e_0 was the thickness measured before the accelerated

test (t=0 h). The evolution of ΔR_s with time is given in Fig. 6B. The average thickness ΔR_s evolution (in micrometers) during accelerated tests was about: $\Delta R_s = 0.58t$ with t the time in hours.

These analyses were completed by SEM-EDS images (Figs. 7 and 8): Rust layer was always confined at the interface between the steel rebar and the mortar and mixed layer was sometimes observed. A white trace was observed in the rust layer (Fig. 7C), which had been attributed to the original trace of the steel rebar in [9].

Distribution of O, Ca, Si and Fe elements was recorded in the rebar/mortar interface of E45 sample (Fig. 8). Corrosion patterns were similar for E10 sample. The layer close to the steel contained mainly iron and oxygen (with low concentrations of calcium, but no siliceous). The presence of iron and oxygen showed that it was the rust layer. Next, a mixed layer had been identified, containing elements coming from the rust layer (iron, oxygen), but also from the mortar (calcium, siliceous). A very little amount of iron element was observed in the mortar far from the observed layers.

Moreover, XRD analysis (Fig. 9) has been made on dried iron oxides. The results revealed that the rust layer was mainly composed of iron oxy-hydroxides (goethite and akaganeite) with also some magnetite.

Calcium element was sometimes observed by EDS in the corrosion layer formed during accelerated tests. Similar observations had been done under natural corrosion but it may be due to an acidification of the solution near steel rebar inducing the dissolution of portlandite. This acidification could induce an additional corrosion as mentioned by [5].

According to these observations, the following corrosion pattern (Fig. 10) was mainly characterized by: metallic substrate, rust layer, and mortar. A mixed layer composed of rust and mortar was sometimes identified. This pattern can be compared to the long term patterns encountered on historical buildings [13]. Authors had found a first layer called “dense product layer” next to the rebar, and a mixed layer called “transformed medium”, containing elements coming from the dense product layer and from concrete. Thus, the observed corrosion pattern is similar with what is obtained under natural corrosion.

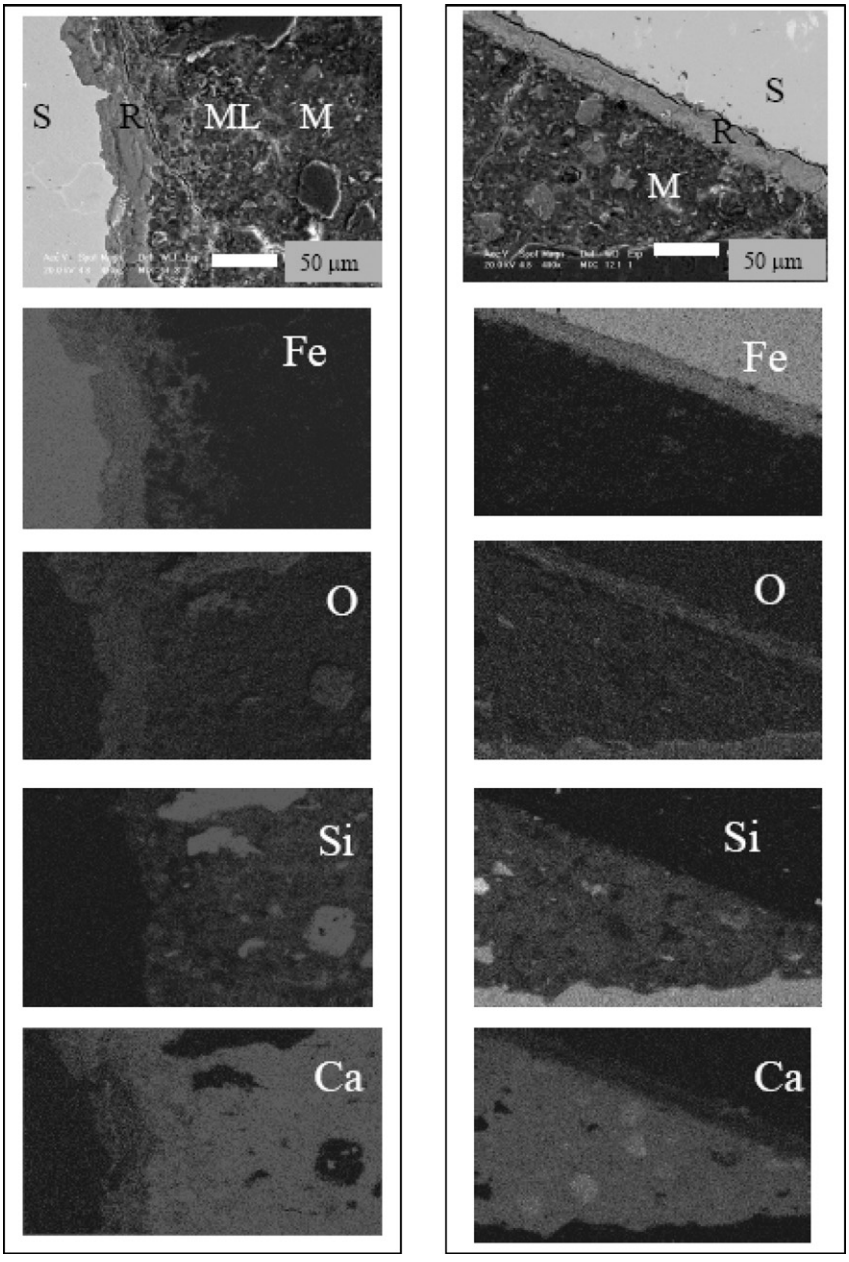

Fig. 8. Elements distribution by EDS for steel/mortar interface for sample E45: SEM, Fe (Iron), O (oxygen), Si (silicon) and Ca (calcium). S: steel, R: rust layer, ML: mixed layer, M: mortar.

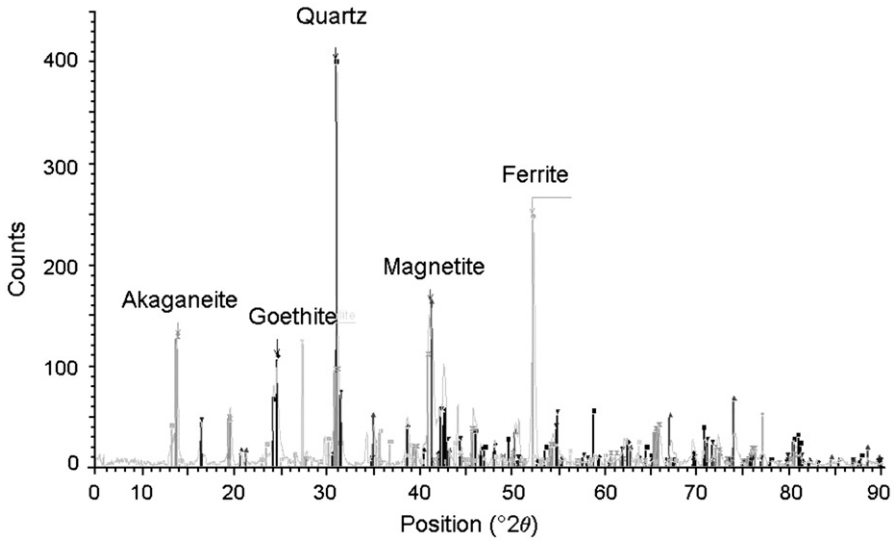

Fig. 9. XRD spectra of rust layer. Rust products composed of iron oxy-hydroxides (goethite and akaganeite) with some magnetite and exogenous elements (Quartz and Ferrite) coming from rebar and mortar.

3.2. Determination of the experimental rust expansion coefficient

The rust expansion coefficient, η, between the volume of expansive corrosion products and the volume of iron consumed in the corrosion process is used in numerical model where pressure induced by the rust layer is modelled by a fictitious thermal load [7]. Theoretical expansion coefficients are usually considered. They are evaluated from the molecular volumes of iron and corrosion products ([14,15]). But the expansion coefficients of the corrosion products formed during accelerated corrosion tests may be different from the theoretical expansion coefficients because of the presence of mortar (confinement of the rust layer). Furthermore the exactly composition of rust layer is not well known, so that it is difficult to determine its molecular volume or its density. For instance, the presence of water in rust products may modify their density and so their expansion coefficient.

In order to estimate the ratio, η, a modelling approach was developed considering rust confined at the interface between steel and mortar (Fig. 11). In this model, we supposed that the reinforcing bar of initial radius R_0 was embedded in cylindrical sample composed of mortar with radius R_3. The radius R_3 was measured from the centre of the bar to the nearest surface of mortar cover.

Assuming uniform corrosion on the bar surface, the radius loss of the steel (or the attacked penetration depth) was defined as X. Then the remaining radius of the bar R_1 was given by $R_1 = R_0 - X$. The radius loss X was evaluated by the Faraday's law according to:

$$X = \frac{M_{Fe} \cdot J_{corr} \cdot \Delta t}{\rho_{Fe} \cdot n \cdot F} \quad (1)$$

with

M_{Fe}	the atomic mass of Fe ($56 \cdot 10^{-3}$ kg/mol),
ρ_{Fe}	the specific weight of Fe (7800 kg/m^3),
n	the valence of Fe (n=2 or 3),
F	the Faraday's number (96500 °C/mol),
J_{corr}	the corrosion current density (100 μA/cm^2=1 A/m^2)
Δt	the test period (s).

As iron oxy-hydroxides have been found in the corrosion product layer, we can consider in the following that n is equal to 3. Furthermore, the Faraday's law is supposed to be valid. That means that a 100% current efficiency [4] is assumed i.e. all the current is spent in the dissolution of iron and no other kind of spontaneous corrosion process is developing during the test, as mentioned above by acidification of the solution.

Thus, for this study, X (in μm) is equal to:

$$X = 0.089\, t \quad (2)$$

with t the time in hours.

The corresponding volume of the steel consumed/unit length (ΔV_s) of the bar is given by:

$$\Delta V_s = \pi R_0^2 - \pi R_1^2 \approx 2\pi \cdot X \cdot R_0 \quad (3)$$

with $X \ll R_0$ and $(R_0 + R_1) \approx 2\, R_0$.

When rust is formed at the interface between steel rebar and mortar, it is possible to determine the radius R_2 where $R_2 = R_1 + \Delta R_s$. Assuming that there is no diffusion of rust in mortar (which was not always the real case), the corresponding volume of accumulated rust products (ΔV_r) around the bar is given by:

$$\Delta V_r = \eta \Delta V_s \quad (4)$$

with η the ratio between the rust volume and the original steel.

ΔV_r is given by:

$$\Delta V_r = \pi R_2^2 - \pi R_1^2 \approx 2\pi \cdot R_0 \cdot \Delta R_s. \quad (5)$$

with $\Delta R_s \ll R_0$ and $(R_0 + R_2) \approx 2\, R_0$.

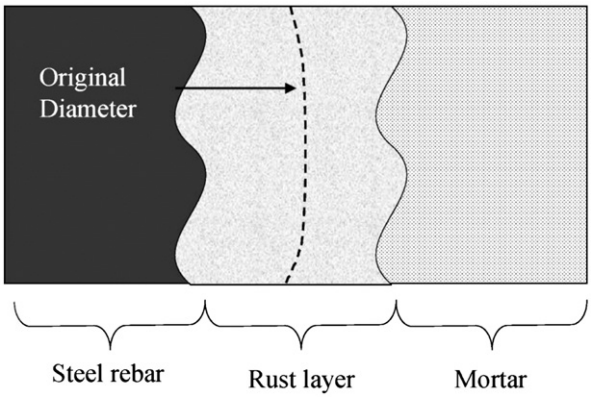

Fig. 10. Schematic section of a steel reinforcement corroded by the impressed current method: metal, dense product layer and mortar.

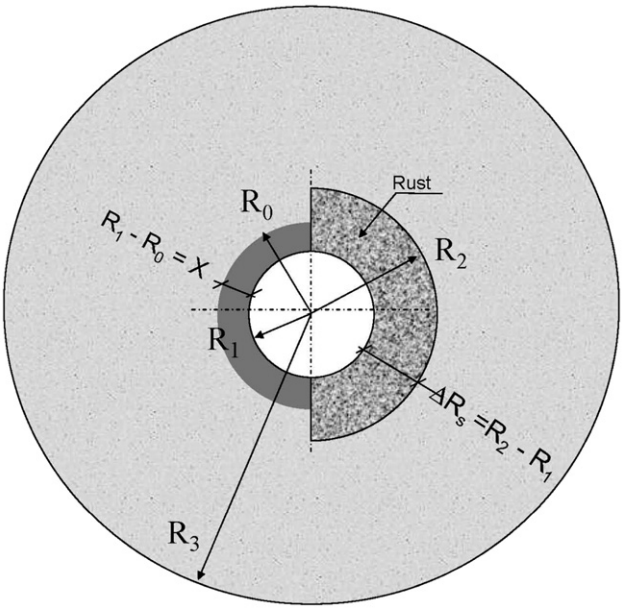

Fig. 11. Geometrical characteristics of the three domains (steel, rust layer, mortar). With R_0: Initial radius of steel rebar. R_1: Radius of steel rebar after corrosion, $R_1 = R_0 + X$ with X the radius loss. R_2: $R_2 = R_1 + \Delta R_s$. R_3: Radius of the specimen.

The ratio η was estimated from Eqs. (2)–(5) according to:

$$\eta = \frac{\Delta R_s}{X}. \quad (6)$$

Considering the average thickness ΔR_s evolution, the ratio η was estimated to be equal to 6.5. As the corrosion pattern is heterogeneous around the rebar (the thickness ΔR_s ranged between $0.13t$ and $1.02t$), the ratio η ranged between 1.5 and 11.4 for $n=3$ (Table 3). These values depend on the assumptions made in the modelling, on the one hand they may be overestimated because of the assumption of 100% current efficiency and on the other hand they may be underestimated because of the "dispersion" of some of the iron oxides into the mortar.

These experimental expansion coefficients were compared with the theoretical values (Table 4) for known corrosion products. The theoretical ratios η were evaluated from the molecular volume V_M of iron and corrosion products according to $V_M = M/\rho$ with M the molecular weight and ρ the specific weight given in [16]. The average predicted value η is superior to the theoretical value η of the corrosion products determined by XRD (goethite, akaganeite) but is coherent with the theoretical value of rust composed of $Fe(OH)_3$ and other hydrated iron hydroxides (see Table 4 for $Fe(OH)_3$, $3H_2O$).

The predicted expansion coefficient allowed determining the density current before accelerated corrosion tests. Assuming a ratio η equal to 6.5, we evaluated the radius loss considering the average thickness of rust equal to 12.5 µm. The radius loss was equal to about 2 µm so that the density current was estimated to about 0.5 µA/cm^2 for samples of 6 months old (around 5 µm/year). This value is in accordance with values estimated in the archaeological analogues studies [13] where average corrosion rates where estimated to be around 5 µm/year.

Table 3
Experimental ratio $\eta = \frac{\Delta R_s}{X}$ for $n=3$

ΔR_s	η for $n=3$
$1.02t$	11.4
$0.58t$	6.5
$0.13t$	1.5

Table 4
Theoretical η ratio between the volume of expansive corrosion products (V_{rust}) and the volume of iron consumed during the corrosion process (V_{Fe})

		Density [16] (kg/m^3)	Molecular weight kg/mol	V_{rust}/V_{Fe}	V_{rust}/V_{Fe} [14,15]
Iron	Fe	7800	0.056	/	/
Hematite	1/2 Fe_2O_3	5260	0.16	2.12	2.2
Magnetite	1/3 Fe_3O_4	5180	0.232	2.08	2
Goethite	α-FeOOH	4260	0.089	2.91	
Akageneite	β-FeOOH	3560	0.089	3.48	
Lepidocrocite	γ-FeOOH	4090	0.089	3.03	
	$Fe(OH)_2$				3.75
	$Fe(OH)_3$				4.2
	$Fe(OH)_3$, $3H_2O$				6.40

3.3. Concluding remark

Microstructural observations by OM and SEM showed that the corrosion pattern induced by impressed current was mainly characterized by a rust layer confined at the interface between the steel and the mortar. This layer was mainly composed of iron oxy-hydroxides and its thickness ΔR_s varied linearly with time according to $\Delta R_s = 0.58t$ with t the time in hours. Mixed layer was sometimes observed.

Furthermore, a modelling analysis showed that the volume of rust products was about 6.5 times the volume of iron. The predicted expansion coefficient is in accordance with rust layer composed of iron oxy-hydroxides and water.

This volume increase is the principal cause of the expansion and ultimately the cover cracking. The aim of our mechanical measurements was to verify this hypothesis.

4. Mechanical effects of rust layer

4.1. Experimental displacement field measurements at steel/mortar interface

During the accelerated corrosion test, we observed crack initiation around the steel rebar after about 15 h. Cracks propagated through the mortar cover and open to the surface after 41 h. Furthermore, the intercorrelation image technique allowed determining different stages during the corrosion process.

Fig. 12 gives the radial displacement (along axis 1) after 1 and 3.5 h for the zone observed with the CCD camera. As long as the corrosion products filled the porous zone at steel/mortar interface no significant pressure was created on mortar, and the displacement field was continuous (the radial displacement was the same in steel and mortar in Fig. 12A). After 3.5 h, the radial displacement was higher in mortar (Fig. 12B) that means that the radial displacement was no longer continuous across the interface. It means that a pressure was created by the corrosion products that had filled the porosity of the interface zone. Therefore, the time necessary for the rust to induce pressure on the mortar in this test can be estimated to 3.5 h.

Furthermore the relative displacement that was determined between two points (P_1 on the mortar and P_2 on the steel as shown in Fig. 3 and in Fig. 12) is represented on Fig. 13. The distance between the points P_1 and P_2 was about 94 µm. The radial displacement $U(r=d(P_2-P_1)=94\ \mu m)$ along axis 1 was much more important than the one along axis 2 close to zero. The radial displacement increased with time up about 15 h and after 15 h it was constant ($U(r) \approx 1$ µm/h). This time corresponds to time to cracking, that means that cracking may modify the corrosion effect. Before the time to cracking, the radial displacement varies linearly with time according to:

$$U(r = d(P_2 - P_1) = 94\mu m) = 0.071\, t \quad (7)$$

with t in hours and $U(r=d(P_2-P_1)=94\ \mu m)$ in micrometers.

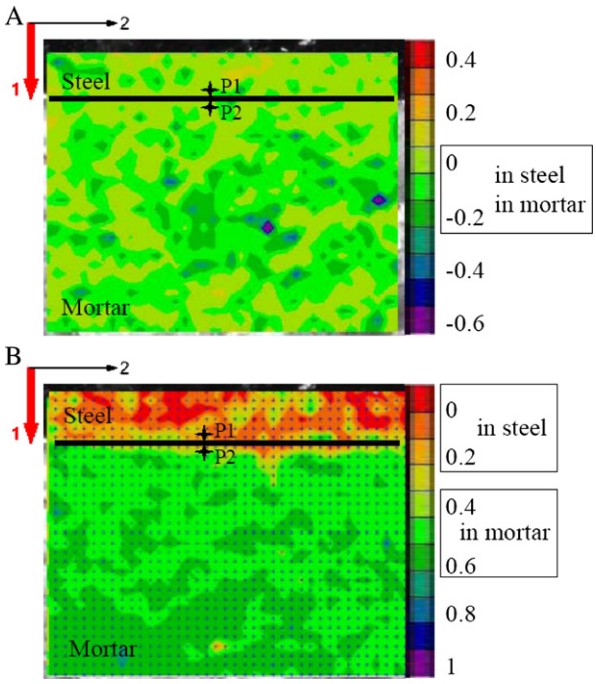

Fig. 12. Radial displacement after 1 h and 3.5 h obtained by using digital image correlation (in pixel with 1 pixel=0.95 μm).

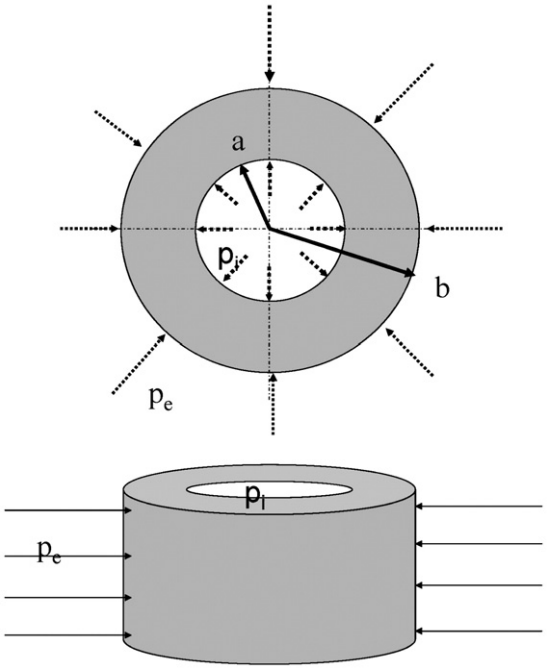

Fig. 14. Model of the hollow cylinder subjected to inner pressure P_i and outer pressure P_e, with inner radius a and outer radius b.

The observed zone may be not representative of the overall corrosion process around the steel rebar because the rate of radial displacement of the mortar can be variable of one at the other zone. Nevertheless, the displacement field was homogeneous around the rebar before cracking (Fig. 12). Moreover, the radial displacement given by another test had the same order of magnitude ($U(r)\approx 0.064t$). In the following the radial displacement along axis 1 was assumed to be the same around the rebar ($U(r)\approx 0.071t$) and the orthoradial displacement along axis 2 was neglected.

4.2. Analytical corrosion model

The data on the evolution of the thickness and on the displacement of the mortar in the observed zone allowed calibrating the time to cracking and the Young's modulus of rust in the reinforced mortar using an analytical model (hollow cylinder subjected to pressures).

4.2.1. Modelling problem

In order to predict the mechanical behaviour of reinforced mortar subjected to corrosion, it is important to model, in a realistic way, the behaviour of (i) mortar itself, (ii) steel rebar and also (iii) corroded steel layer. In this study, the problem was modelled with reference to Fig. 14. We considered a hollow cylinder composed of a solid phase subjected to inner pressure P_i and outer pressure P_e as described in [17]. The inner radius was noted $r=a$ and the outer radius was noted $r=b$. The solid phase was a linear, homogeneous and isotropic material, characterized by the Lamé constants. Furthermore, it was assumed that $\sigma_z=0$.

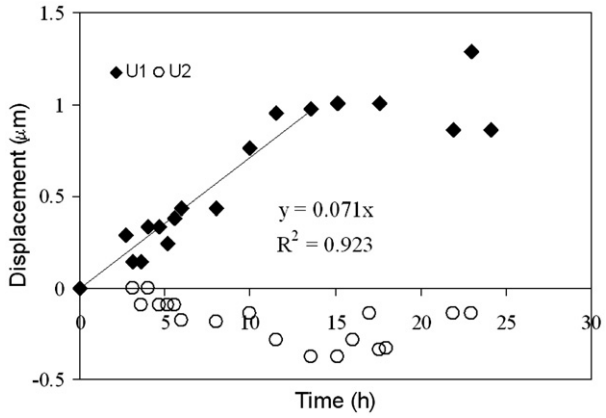

Fig. 13. U1 (μm): Radial displacement along axis 1 and U2 (μm): displacement along axis 2 versus time (h). Relationship between the displacement U1 and the time t for time less than 15 h.

In the cylindrical coordinates system, the radial displacement $U(r)$ is given by:

$$U(r) = C_1 \cdot r + \frac{C_2}{r} \tag{8}$$

where r is the radius which varies between a and b and C_1 and C_2 are two constants defined as:

$$C_1 = \frac{1-\nu}{E} \cdot \frac{a^2 \cdot p_i - b^2 \cdot p_e}{b^2 - a^2} \tag{9}$$

$$C_2 = \frac{1+\nu}{E} \cdot \frac{a^2 \cdot b^2 \cdot (p_i - p_e)}{b^2 - a^2} \tag{10}$$

where ν and E are the mechanical properties of the hollow cylinder (Poisson's ratio and Young's modulus).

In the cylindrical coordinates system, the radial stress σ_r and the orthoradial stress σ_t are given by:

$$\begin{aligned}\sigma_r &= \frac{E}{1-\nu^2}\left(C_1 \cdot (1+\nu) - C_2 \cdot \frac{1-\nu}{r^2}\right) \\ &= \frac{a^2 \cdot p_i - b^2 \cdot p_e}{b^2 - a^2} - \frac{a^2 \cdot b^2 \cdot (p_i - p_e)}{r^2 (b^2 - a^2)}\end{aligned} \tag{11}$$

$$\begin{aligned}\sigma_t &= \frac{E}{1-\nu^2}\left(C_1 \cdot (1+\nu) + C_2 \cdot \frac{1-\nu}{r^2}\right) \\ &= \frac{a^2 \cdot p_i - b^2 \cdot p_e}{b^2 - a^2} + \frac{a^2 \cdot b^2 \cdot (p_i - p_e)}{r^2 (b^2 - a^2)}.\end{aligned} \tag{12}$$

In order to evaluate the mechanical effect generated by reinforcement bar corrosion, this model was applied in two cases:

- The hollow cylinder was composed of mortar (cases A and B). This hypothesis allowed us to determine the time to cracking t_c. This model was compared with analytical modelling proposed by authors ([14,15,18–20]).
- The hollow cylinder was composed of the rust layer (cases C and D). This hypothesis allowed us to determine the Young's modulus of rust.

For these two cases, two hypotheses have been made. Firstly, it was supposed that the radius of the rebar and the thickness of the rust were the same during the accelerated corrosion test (cases A and C). Secondly, the evolution of the rebar radius and the thickness of the rust have been taken into account (cases B and D). The first hypothesis corresponds to hypothesis made in numerical modelling ([6,7]) and the second hypothesis allows being more realistic.

4.2.2. Evaluation of cracking time

In order to predict the time to cracking t_c, the hollow cylinder was assumed to be composed of mortar. The inner radius was noted $r=a$ and the outer radius was noted $r=b$. In this case, the tensile stress at the radius $r=a$ was estimated from Eq. (12) when the pressures P_i and P_e are known. The outer pressure P_e was supposed to be equal to the atmospheric pressure ($P_e=0.1$ MPa).

This model was applied in two cases A and B:

- Model A: The radius $r=a$ was assumed to be constant during the accelerated corrosion test. In this case the inner radius $r=a$ was equal to $a=R_0+e_r$ where R_0 was the initial radius of steel rebar and e_r was the thickness of the rust layer supposed to be equal to 30 μm. This value corresponded to the thickness of the rust at $t=15$ h (experimental time to cracking) as shown in Fig. 6A.
- Model B: The model was used with $a=R_1+\Delta R_s$ as defined in Fig. 11. $R_1=R_0-X$ with X the radius loss given by the Faraday's law (with $n=3$) and ΔR_s was estimated from the OM observations ($\Delta R_s=0.58t$). Thus, the effects of corrosion on upper surface of the mortar were assumed to be similar to the ones in the inner reinforced mortar.

For the two models (A and B), the outer radius was equal to $b=R_3$ and we supposed that there was no initial corrosion at $t=0$ (before the accelerated corrosion test), i.e. $R_0=5$ mm.

For these two cases (A and B), the inner pressure P_i was determined from Eqs. (7) to (8). Then, the orthoradial stress σ_t was deduced from Eq. (12). This result showed that the inner pressure P_i and the orthoradial stress σ_t vary linearly with time (Figs. 15 and 16) and are

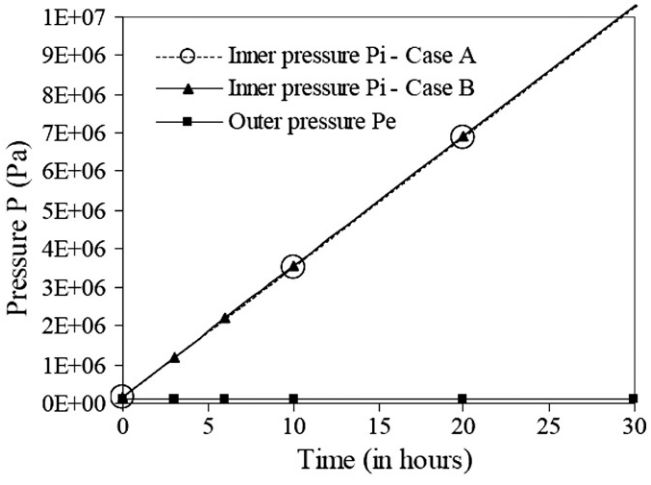

Fig. 15. Inner pressure P_i versus time (for the two models A and B according to Eqs. (7) and (8)) and outer pressure P_e versus time.

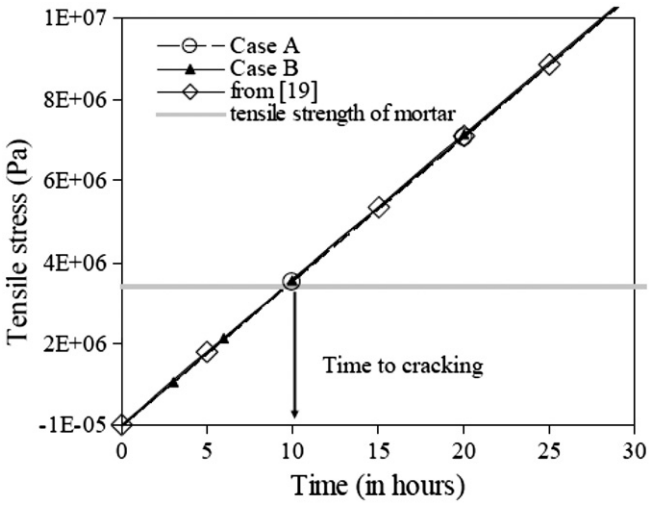

Fig. 16. Tensile stress against time for the different model and prediction of the time to cracking.

the same order of magnitude for the two models (model A and model B). Thanks to these models the displacement U_i at $r=a$ with $U_i=U(r=a)>U(r=d(P_2-P_1)=94$ μm) and the orthoradial stress σ_t at $r=a$ were evaluated.

The results show that the radial stress σ_t can be neglected ($\sigma_r \approx 10^{-3}\,\sigma_t$) so that the stress field may be assumed to be unidirectional. Thus the time to cracking t_c may be deduced assuming that mortar is damaged when the orthoradial stress σ_t is equal to the tensile strength of mortar (3.3 MPa).

For the two models, the time to cracking t_c was about 10 h. This predicted time is in accordance with the experimental time (15 h) but is lower because the model does not take into account the time necessary to fill the mortar porosity during the accelerated corrosion test.

The time to cracking t_c is the same for the two models (A and B) if we take into account the initial corrosion due to the curing step with a radius loss evaluated to 3 μm ($R_0=5$ mm−3 μm). Furthermore, the predicted time to cracking is the same for e_r equal to 0 μm or 60 μm for the case A (Fig. 17). These results showed that the time to cracking t_c does not depend on the value of the thickness of rust layer e_r. Nevertheless, the predicted time to cracking is very sensitive to the value of the radial displacement at the interface between rust and the mortar (Fig. 17). This dependence may be due to the composition of rust products, i.e. to their density.

To validate these results, time to cracking was determined with models proposed by other authors.

Our modelling was first compared to the model proposed by Piltner and Monteiro [18] in which the time to fill the porous zone is not taken into account. In this model, the tensile stress at the corrosion products–mortar interface $r=R_0$ is given by:

$$\sigma_t = 2 \cdot \mu \cdot \frac{p\delta}{r_0} \tag{13}$$

where μ is the shear modulus of mortar ($\mu=12.5$ GPa), $p\delta$ is equal to the displacement $U(r=R_0)$ at the interface between the corrosion products and the mortar with p a "coefficient of expansion" which relates the penetration of corrosion δ (X for us) to the expansion of the corrosion products (see Fig. 18).

We supposed that $R_0=R_1+\Delta R_s$ and $U(r=R_0)$ was given by the radial displacement $U(r=d(P_2-P_1)=94$ μm) measured by the inter-correlation image technique. The "coefficient of expansion" p was estimated to be equal to $8\cdot10^{-7}$. Result of tensile stress is given in Fig. 16. With this model, the predicted time to cracking is also 10 h and is in accordance with our modelling.

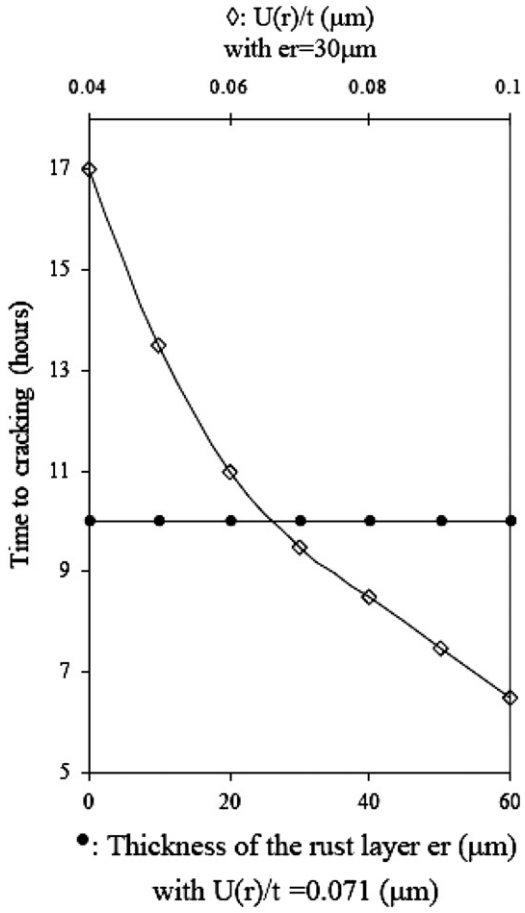

Fig. 17. Influence of the thickness of the rust layer e_r and the radial displacement $U(r)$ at the interface $r=a$ on the time to cracking (model A).

Other authors proposed analytical models which take into account the time to fill the porous zone between steel and mortar. Our experimental data have been applied to these models.

Morinaga ([19] given in [20]) proposed an empirical equation based on field and laboratory data to predict the time from corrosion initiation to corrosion cracking according to:

$$T_{cr} = 0.602D(1+2C/D)^{0.85}/i_{cor} \quad (14)$$

where T_{cr} is the time from corrosion initiation to corrosion cracking (days), D is the steel bar diameter (mm), C is the clear mortar cover (mm) and i_{cor} is the corrosion rate (10^{-4} g/cm^2/day). With our experimental data the predicted time is about 26.5 h.

Maaddawy and Soudki [20] proposed a model which accounts for the time required for corrosion products to fill a porous zone around the steel reinforcing bar before they start inducing expansive pressure on the surrounding mortar. This model depends on the geometrical and mechanical characteristics of the sample (diameter of rebar, thickness of cylinder, Young's modulus and Poisson's ratio of mortar), on the current density and on the thickness of the porous zone δo. The thickness δo of the porous zone is typically in the range of 10–20 μm. With our experimental data, the time to cracking is estimated to 34 h for $\delta o = 10$ μm and 68 h for $\delta o = 20$ μm.

Liu and Weyers [14] or Bhargava et al. [15] proposed a model which considers the critical amount of corrosion products needed to fill the interconnected void space (δo) around the reinforced bar and to generate sufficient tensile stresses to crack the cover mortar. With our data, the time to cracking was estimated to 56 h for akaganeite and with $\delta o = 10$ μm [14].

These predicted times to cracking are higher than our predicted value (10 h). Nevertheless, in our tests, it should be necessary to add the time before the corrosion accelerated test (i.e. during the curing step). So, for specimens of 6 months old and with a current density estimated to 0.5 μA/cm^2 the "true" time to cracking should be evaluated to:

$$t'_c = t_c + 365/2/200*24 = 10 + 22 = 32 \text{ hours}. \quad (15)$$

This predicted time t'_c is coherent with the models which take into account the time to fill the porous zone between steel and mortar.

4.2.3. Estimation of mechanical properties of rust

The main difficulty in numerical modelling lies in the determination of the parameters of the interface, in term of Young's modulus and Poisson's ratio to reproduce the development of corrosion. We used the model of the hollow cylinder subjected to inner and outer pressures to calibrate the Young's modulus of rust. In this case, we supposed the hollow cylinder to be composed of the rust layer. In this model, the Poisson's ratio was assumed to be 0.3 equal to the Poisson's ratio of steel.

This model was applied in two cases:

- Model C: The radii $r=a$ and $r=b$ were the same during the accelerated corrosion test. In this case, the inner radius $r=a$ was supposed to be equal to $a=R_0$ where R_0 is the initial radius of the steel rebar. The outer radius $r=b$ was supposed to be equal to $b=R_0+e_r$ where e_r is the thickness of the rust layer equal to $e_r=30$ μm.

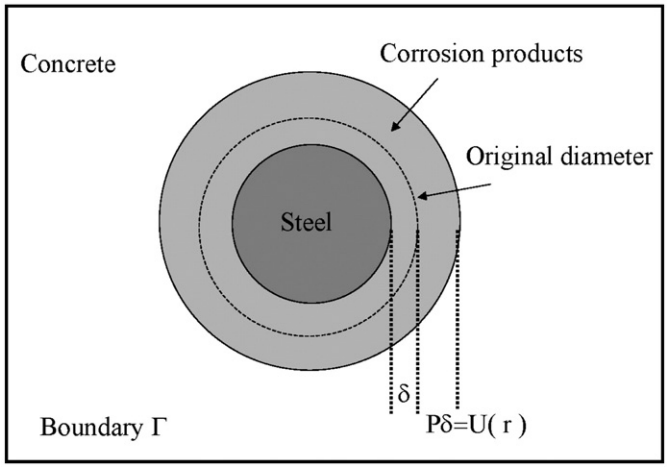

Fig. 18. Model used by [18] to estimate the stresses developed during the corrosion of reinforced concrete.

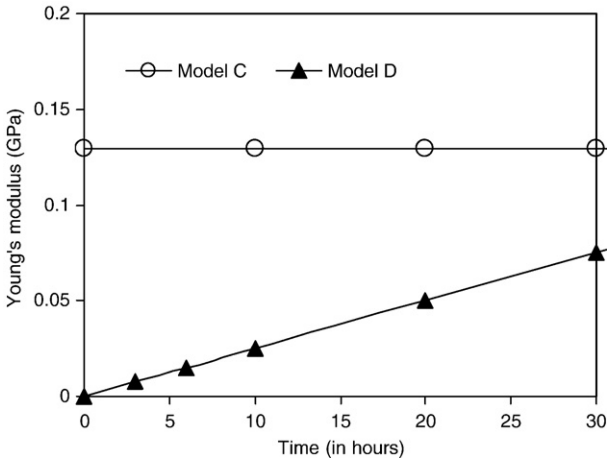

Fig. 19. Young's modulus of rust layer against time for the two models C and D.

- Model D: The model was used with $a=R_1$ as defined in Fig. 11. The outer radius $r=b$ was equal to $b=R_1+\Delta R_s$ to take into account the evolution of the radii with time during accelerated corrosion test.

For the two models (C and D), we determined the constants C_1 and C_2 from Eq. (7) to (8) assuming that $U(r=a)=0$ and $U(r=b)=U_i$ deduced from models A or B. Then, the Young's modulus was deduced from Eq. (11) assuming that the radial stress was equal to $\sigma_r=-P_i$ with the pressure P_i determined in the cases A or B.

The calibrated Young's modulus is given in Fig. 19. For the first case (model C), it is constant and equal to 0.13 GPa. For the second case (model D), the predicted Young's modulus is less and varies linearly with time. It can be noticed that the calibrated value depends on the Poisson's ratio of rust. For instance, the Young's modulus is equal to 0.14 (with model C) if the Poisson's ratio is equal to 0.2.

The result for the Young's modulus (Fig. 20) is the same whatever the value of the radial displacement at the interface between the rust and the mortar $U(r)$, but the result depends on the initial value of the thickness e_r of the rust (or of the initial radius R_0). This result is coherent with the dependence of the Young's modulus with time for the model D. This dependence may be due to the compaction of the layer under the effect of the confinement.

4.3. Concluding remark

Displacement field at the interface between steel and mortar was determined by using digital image correlation. Our result showed that the radial displacement at the interface rust/mortar is about $U(r)\approx 0.07t$.

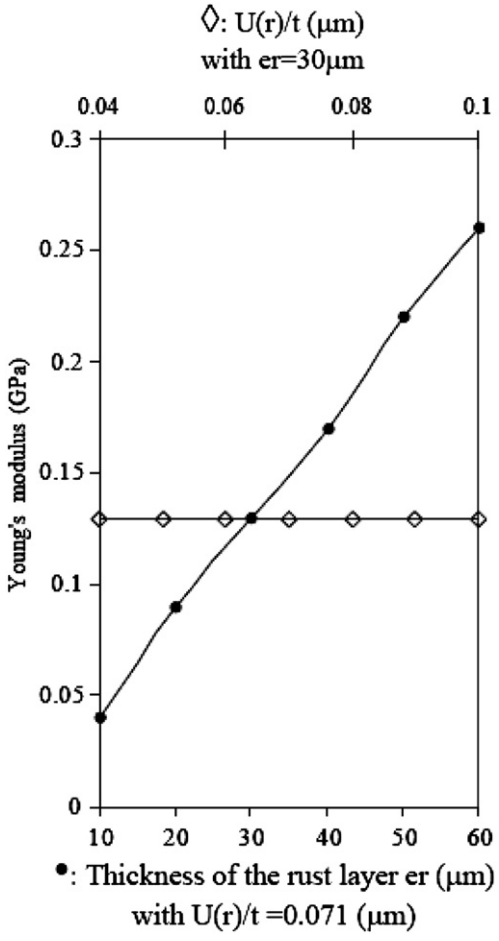

Fig. 20. Influence of the thickness of the rust layer e_r and the radial displacement $U(r)$ at the interface $r=a$ on the Young's modulus of the rust (model C).

This datum allowed predicting the time to cracking and the Young's modulus of rust by using the analytical model of hollow cylinder subjected to inner and outer pressures. Our modelling showed that the predicted time to cracking does not depend on the thickness of the rust layer but it depends on the displacement of the interface steel/mortar. This model did not allow to take into account the time to fill the porous zone. Concerning the Young's modulus, our results showed that the calibrated value depends on the thickness of the rust layer e_r and then on the geometrical characteristics of the mechanical modelling.

5. Conclusions

The aim of this study was to analyse the mechanical effects of corrosion products on the cracking of mortar. Accelerated corrosion tests by impressed current method were performed to determine the corrosion pattern and the displacement field by using digital image correlation.

The results obtained showed that:

- Under accelerated tests rust layer was formed at the interface steel/mortar. This phase was mainly composed of iron oxy-hydroxides and its thickness ΔR_s varied linearly with time.
- Under accelerated tests rust layer was formed at the interface steel/mortar. This phase was mainly composed of iron oxy-hydroxides and its thickness ΔR_s varied linearly with time.
- The radial displacement at the interface rust/mortar was evaluated by using digital image correlation. It varied linearly with time for times t inferior to about 15 h, i.e. before the time to cracking.

The analytical model of a hollow cylinder subjected to inner and outer pressures allowed predicting the time to cracking and calibrating the Young's modulus of the rust layer from the value of the radial displacement of the interface steel/mortar. The time to cracking depends on the radial displacement value. With this model the time to cracking was underestimated because this model did not to take into account the time to fill the porous zone between steel and mortar.

This modelling allowed calibrating the Young's modulus too. Our results showed that the calibrated Young's modulus of the rust layer depends on the thickness of the rust and on the initial radius of the reinforcement. Consequently the value of the Young's modulus used in numerical modelling depends on the geometrical characteristics (radius of the steel and thickness of the rust layer). For instance, in the case where the reduction of the rebar diameter is taken into account in numerical modelling, Young's modulus can't be considered as constant.

There is still a need for more experiment results to predict the mechanical properties of rust in reinforced concrete structures without calibration and to better understand the effect of the confinement of the rust layer on the mechanical properties This implies numerous experiments and a lot of different measurements (mechanical, geometrical, electrochemical…) on simple structures to analyse the development of corrosion, its mechanical effects and the final products. It would be interesting to have a better knowledge of the rust composition (valence number of iron, density of rust) in order to predict the thickness evolution of rust and the expansion coefficient.

Moreover, this study has to be extended to the case of natural corrosion and it would be interesting to study the influence of the mixed layer on the mechanical effects. More attention has to be paid to the porous zone between steel and mortar to improve the time to cracking too.

Acknowledgments

This work has been supported by CEA (CIMETAL program), EDF (Electricité de France) and LCPC (Laboratoire Central des Ponts et Chaussées).

SEM observations were performed at the Laboratory LCPC. XRD have been performed at CEA by William Guillot.

References

[1] K. Tuutti, Corrosion of steel in concrete, Swedish Cement and Concrete Research Institute, Stockholm, 1982.
[2] A. Pourbaix, V. L'Hostis, Passivation, localised corrosion and general corrosion of steel in concrete and bentonite, Theory and Experimentals, Proceedings of the NUCPERF 2006 Workshop, Cadarache, France (27–30 Mars 2006), Journal de Physique IV, vol. 136, 2006, pp. 71–78.
[3] D.J. Anstice, C.L. Page, M.M. Page, The pore solution phase of carbonated pastes, Cement and Concrete Research 35 (2005) 377–383.
[4] C. Andrade, C. Alonso, F.J. Molina, Cover cracking as a function of bar corrosion: part I — experimental test, Materials and Structures 26 (1993) 453–464.
[5] C. Alonso, C. Andrade, J. Rodriguez, J.M. Diez, Factors controlling cracking of concrete affected by reinforcement corrosion, Materials and Structures 31 (1998) 435–441.
[6] F.J. Molina, C. Alonsi, C. Andrade, Cover cracking as a function of rebar corrosion: part 2 — numerical model, Materials and Structures 26 (1993) 532–548.
[7] Q.T. Nguyen, S. Caré, A. Millard, Y. Berthaud, Analyse de la fissuration du béton armé en corrosion accélérée, C. R. Mecanique 335 (2007) 99–104.
[8] A. Ouglova, M. François, Y. Berthaud, S. Caré, F. Foct, Mechanical properties of an iron oxide formed by corrosion in reinforced concrete structures, Proceedings of the NUCPERF 2006 Workshop, Cadarache, France (27–30 Mars 2006), Journal de Physique IV, vol. 136, 2006, pp. 99–107.
[9] S. Caré, A. Raharinaivo, Influence of impressed current on the initiation of damage in reinforced mortar due to the corrosion of embedded steel, Cement and Concrete Research 37 (2007) 1598–1612.
[10] F. Hild, J.N. Périé, M. Coret, Mesure de champs de déplacements 2D par corrélation d'images numérique 2D, Rapport interne, LMT-ENS, Cachan, 1999, in French.
[11] S. Roux, F. Hild, Y. Berthaud, Correlation image velocimetry: a spectral approach, Applied Optics OT41 1 (2002) 108–115.
[12] Q.T. Nguyen, Étude expérimentale et théorique de l'effet de la corrosion sur la fissuration et le comportement global des structures en béton armé, Thèse de Doctorat, Université Pierre et Marie curie (UPMC), 2006, in french.
[13] W.J. Chitty, P. Dillmann, V. L'Hostis, C. Lombard, Long term corrosion resistance of metallic reinforcements in concretes — a study of corrosion mechanisms based on archaeological artefacts, Corrosion Science 47 (6) (2005) 1555–1581.
[14] Y. Liu, R.E. Weyers, Modeling the time-to-corrosion cracking in chloride contaminated reinforced concrete structures, ACI Materials Journal 95-M65 (1998) 675–681.
[15] K. Bhargava, A.K. Ghosh, Y. Mori, S. Ramanujam, Modeling of time to corrosion-induced cover cracking in reinforced concrete structures, Cement and Concrete Research 35 (2005) 2203–2218.
[16] U. Schwertmann, R.M. Cornell, Iron Oxides in the Laboratory, Preparation and Characterization, VCH, 1991.
[17] S.P. Timoshenko, J.N. Goodier, Theory of elasticity, 3rd ed.Mc Graw-Hill book Compagny, New York, 1970.
[18] R. Piltner, P.J.M. Monteiro, Stress analysis of expansive reactions in concrete, Cement and Concrete Research 30 (2000) 843–848.
[19] S. Morinaga, Prediction of service lives of reinforced concrete buildings based on rate of corrosion of reinforcing steel, Report No23, Shimizu Corp, Japan, 1988, p. 82.
[20] T.El. Maaddawy, K. Soudki, A model for prediction of time from corrosion initiation to corrosion cracking, Cement and Concrete Composites 29 (2007) 168–175.